Dyes and Pigments 120 (2015) 37–43

Contents lists available at ScienceDirect

Dyes and Pigments

journal homepage: www.elsevier.com/locate/dyepig

Synthesis of a water soluble red fluorescent dye and its application to living cells imaging

Zheng Gao [a], Xu Zhang [a], Meiling Zheng [b], Yi Chen [a, *]

[a] Key Laboratory of Photochemical Conversion and Optoelectronic Materials, Technical Institute of Physics and Chemistry, The Chinese Academy of Sciences, Beijing 100190, China

[b] Laboratory of Organic NanoPhotonics and Key Laboratory of Functional Crystals and Laser Technology, Technical Institute of Physics and Chemistry, The Chinese Academy of Sciences, Beijing 100190, PR China

ARTICLE INFO

Article history:
Received 12 January 2015
Received in revised form
3 April 2015
Accepted 4 April 2015
Available online 11 April 2015

Keywords:
Dicyanoisophorone derivative
Red fluorescent dye
Stoke's shift
Water-solubility
Synthesis
Living cells fluorescence imaging

ABSTRACT

A water soluble red fluorescent dye (**TD-mPEG$_{750}$**) has been prepared by treatment of 2-(3,5,5-trimethylcyclohex-2-en-1-ylidene)malononitrile with 4-(diethylamino)-2-mPEG benzaldehyde (mPEG-OH, average MW = 750). **TD-mPEG$_{750}$** exhibits red emission at λ_{em} = 664 nm in water, a small fluorescence quantum yield (ϕ_f = 0.01) and a large Stoke's shift ($\Delta\lambda$ = 145 nm) are obtained. Using HeLa cells as prototype, the application of **TD-mPEG$_{750}$** to living cells imaging has been investigated. It is found that **TD-mPEG$_{750}$** can be clearly expressed in mitochondria with high contrast in HeLa cells imaging.

1. Introduction

The use of water-soluble fluorophore dyes has become a significant area of research in biomedical diagnosis and biological image [1–8]. Fluorescent dyes with red emission ($\lambda_{em} \geq 650$ nm) are highly desired in biological imaging due to their particular advantages such as large penetration depth, less light scattering and minimized tissue auto-fluorescence background [9–12]. Common fluorophore dyes such as fluorescein, rhodamine, and quinine sulfate exhibit short emission wavelength ($\lambda_{em} \leq 600$ nm) [13–15], which limited their application in biological imaging. Recently, a number of noted red fluorophore dyes including BODIPY [16–20], cyanine dyes [21–24] and others [25–27] have been developed, but one main problem is encountered with them: small Stoke's shift ($\Delta\lambda \leq 70$ nm).

Development of water-soluble red fluorophore dyes with large Stoke's shift is essential for biological applications [28–31]. Advances in fluorescent dyes with large Stoke's shift not only reduce the self-quenching resulted from the molecular self-absorption due to the overlap between absorption and emission spectral of dyes but also can be used in multiplex monitor since monitoring multiple physiological parameters require the loading of several distinct fluorescent probes in the intracellular and extracellular environments [32], in which fluorophores that are excitable at the same fixed wavelength with well-separated emissions are required.

Dicyanoisophorone derivatives have currently attracted considerable attention because of red emission and large Stoke's shift [33–36]. Herein, a water-soluble fluorescent dye **TD-mPEG$_{750}$** based on dicyanoisophorone system (Scheme 1) has been designed and synthesized. The fluorophore **TD** is easy prepared and shows good photo-stability, the introduction of methyoxypolyethylene glycol (mPEG$_{750}$) to **TD** is to improve the solubility of **TD** in water and to decrease cytotoxicity. Poly(ethylene glycol) (PEG) have been extensively studied for their potential biomedical applications as scaffolds in tissue engineering [37,38] and as drug delivery systems [39,40] due to their biocompatibility, nontoxicity, and biodegradability [41,42]. In this paper, the properties of **TD-mPEG$_{750}$** and its application to cells imaging are examined, some merits are obtained, they include:

- Facile preparation.
- Good solubility in water.

* Corresponding author. Tel.: +86 10 8254 3595; fax: +86 10 6487 9375.
E-mail address: yichen@mail.ipc.ac.cn (Y. Chen).

http://dx.doi.org/10.1016/j.dyepig.2015.04.010
0143-7208/

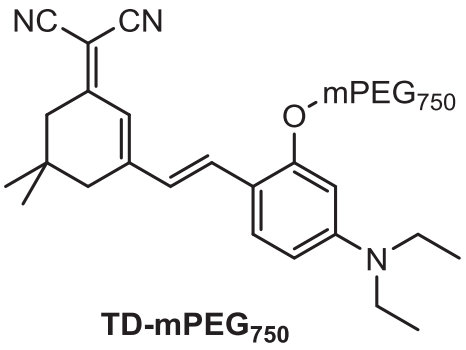

Scheme 1. Chemical structure of **TD-mPEG$_{750}$**.

➢ Deep red fluorescence.
➢ Large stoke's shift.

2. Experimental

2.1. General

^{1}H and ^{13}C NMR spectra are recorded at 400 and 100 MHz, respectively, with TMS as an internal reference. MS spectra are recorded with MALDI-MS spectrometer. UV absorption spectra and fluorescence spectra are measured with an absorption spectrophotometer (Hitachi U-3010) and a fluorescence spectrophotometer (F-2500), respectively. All experiments are carried out with commercially available reagents and solvents, and used without further purification, unless otherwise noted.

2.2. Experiment for cell culture and fluorescence images

For the fluorescence imaging in live cells, HeLa cells are cultured in culture media Dulbecco's modified Eagle's medium (DMEM/F12 1:1 (HyClone) with 10% Fetal Bovine Serum (FBS) and 1% Penicillin-Streptomycin) at 37 °C under a humidified atmosphere containing 5% CO_2 for 24 h. The cells were seeded on a Ø 35 mm glass-bottomed dish (NEST) for live-cell imaging by confocal laser scanning microscopy (CLSM). The HeLa cells were treated with 1 μM of **TD-mPEG$_{750}$** in 2 mL of serum free medium for 2 h and imaged by CLSM without removing the molecule in the cell medium. Confocal fluorescence imaging was performed with Nikon multiphoton microscopy (A1R MP) with a 60 × oil-immersion objective lens (NA = 1.40) and living cell work station. The cellular images were taken under a CLSM by using the excitation channel at 561 nm.

2.3. Experiment for toxicity test

Toxicity test of HeLa cells incubated with **TD-mPEG$_{750}$** is carried out as follows: (a) HeLa cells were incubated with 1 μM of **TD-mPEG$_{750}$** for 2 h, after washed up 3 times with phosphate buffered saline (PBS), 1 mL of fresh PBS was added. (b) To the incubated HeLa cells in PBS was added propidium iodide (PI) probe, after incubation for 10 min, the HeLa cells with **TD-mPEG$_{750}$** and PI probe were washed up with PBS for three times, 500 μL of fresh PBS was then added. (c) The sample was observed by Nikon A1R confocal fluorescence microscope with excitation wavelength of 561 nm, and the range of collected fluorescence is 570–620 nm. (d) The number of dead cells (red) and the whole number of cells were counted from the obtained images. Around 200 cells were counted, and the ratio of living cells (viability, %) was calculated. The viability of the cells without incubation of **TD-mPEG$_{750}$** was also checked by Plunder under the same experimental condition. The viability (%) of stained cells is calculated by relation to that of unstained cells in which the viability of unstained cells is set to 100%.

2.4. Synthesis of *TD-mPEG$_{750}$*

The synthetic route for **TD-mPEG$_{750}$** is outlined in Scheme 2, and the detailed procedures are as follows: (a) To a solution of isophorone (3.8 g, 27.6 mmol) and malononitrile (1.82 g, 27.6 mmol) in dry ethanol (150 mL) was added piperidine (23 mg, 0.276 mmol). The solution was stirred at 60 °C till starting material disappeared (detected by TLC plate). After cooling to room temperature, the solution was slowly poured into water (200 mL) and the precipitated solid was filtered. Recrystallization from heptane afforded 2-(3,5,5-trimethylcyclohex-2-enylidene) malononitrile as a brown solid. Yield: 4.5 g (90%). M.p. 73–75 °C. ^{1}H NMR ($CDCl_3$): δ (ppm) 6.60 (s, 1H), 2.53 (s, 2H), 2.14 (s, 2H), 2.01 (s, 3H), 1.32 (s, 6H). ^{13}C NMR ($CDCl_3$): δ (ppm) 170.3, 161, 120.2, 113.1, 76.4, 45.6, 42.3, 32.4, 27.5, 25.1. (b) To the solution of methoxypolyethylene glycol ($mPEG_{750}$-OH) (7.5 g, 10 mmol) in $CHCl_3$ (30 mL) was added thionyl chloride (2.5 g, 21 mmol) and pyridine (1.6 g, 20 mmol), the solution was refluxed till no starting material was detected (TLC detection). After cooled down to room temperature, the solution was poured into water (100 mL) and extracted with $CHCl_3$ (30 mL × 3). The combined organic solution was dried over Na_2SO_4, after evaporation of the solvent, the product **mPEG$_{750}$-Cl** (oil, 6.5 g, 85% yield) was obtained for next step without purification. (c) To a solution of 4-(diethylamino)-2-hydroxybenzaldehyde (0.96 g, 5 mmol) in DMF (10 ml) was added **mPEG$_{750}$-Cl** (3.8 g, 5 mmol), K_2CO_3 (0.7 g, 5 mmol) and KI (0.08 g, 0.5 mmol). The mixture solution was heated at 100 °C till no starting material was detected (TLC detection). After evaporation of DMF under pressure, 20 ml of H_2O was added to the mixture. The mixture was extracted with DCM (20 mL × 3), the combined organic solution was dried over Na_2SO_4, after evaporation of the solvent, **DA-mPEG$_{750}$** (oil, 2.26 g, 50% yield) was obtained. ^{1}H NMR (400 MHz, $CDCl_3$) δ (ppm) 10.09 (s, CHO), 7.65 (d, J = 8.8 Hz, Ar–H), 6.85–6.81 (m, Ar–H), 6.22 (d, J = 8.8 Hz, Ar–H), 3.81–3.45 (m large, PEG backbone), 3.37–3.32 (q, N–$\underline{CH_2}CH_3$), 3.31 (s, –O–CH_3), 1.14 (t, N–$CH_2\underline{CH_3}$). (d) Under argon, 2-(3,5,5-trimethylcyclohex-2-enylidene) malononitrile (0.46 g, 2.5 mmol) and **DA-mPEG$_{750}$** (2.26 g, 2.5 mmol) were dissolved in dry acetonitrile (10 mL). Piperidine (2.1 mg, 0.025 mmol) was added and the solution was stirred at 40 °C till starting material disappeared (detected by TLC plate). After evaporation of acetonitrile under pressure, 20 ml of H_2O was added to the mixture. The mixture was extracted with DCM (20 mL × 3), the combined organic solution was dried over Na_2SO_4, after evaporation of DCM, the target compound **TD-mPEG$_{750}$** (oil, 2.7 g, 50% yield) was obtained. ^{1}H NMR (400 MHz, $CDCl_3$) δ (ppm) 7.34 (d, J = 8.8 Hz, Ar–H), 7.32 (d, J = 16.0 Hz, CH=CH), 7.02 (d, J = 5.2 Hz, Ar–H), 6.86–6.81 (m, Ar–H), 6.69 (s, Ar–H), 6.24 (d, J = 8.8 Hz, Ar–H), 6.06 (d, J = 2.0 Hz, CH=C), 3.61–3.56 (m large, PEG backbone), 3.37–3.32 (q, $\underline{CH_2}CH_3$), (3.31 (s, –O–CH_3), 2.51 (s, CO–CH_2–), 2.16 (s, –CH_2–), 1.32 (s, CH_3–C–CH_3), 1.14 (t, N–$CH_2\underline{CH_3}$). ^{13}C NMR (100 MHz, $CDCl_3$: δ = 158.3, 155.6, 151.4, 136.7, 134.3, 131.8, 129.0, 128.5, 124.1, 115.3, 113.3, 112.0, 78.3, 78.8, 70.51 (br PEG), 65.4, 57.4, 41.2, 40.3, 37.6, 31.7, 28.1, 14.4. IR (KBr) ν (cm^{-1}) = 3122, 1640, 1589, 1470, 1455, 1240, 1112 (br).

3. Results and discussion

3.1. Synthesis of *TD-mPEG$_{750}$*

TD-mPEG$_{750}$ is obtained from isophorone, malononitrile and the corresponding aromatic aldehydes by a two-step condensation

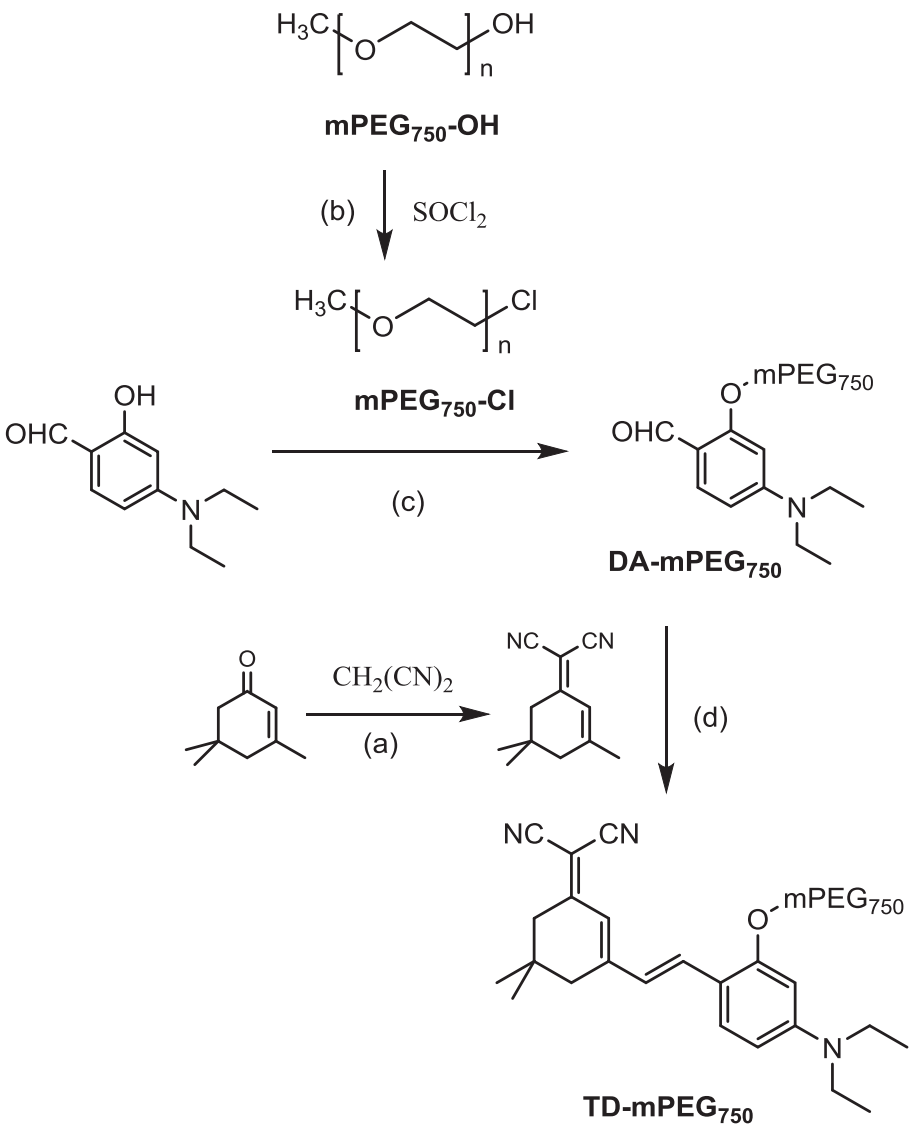

Scheme 2. Synthesis of **TD-mPEG$_{750}$**. Reagents and conditions: (a) piperidine cat., dry EtOH, 60 °C, 90%; (b) pyridine, dry $CHCl_3$, reflux, 85%; (c) KI cat., K_2CO_3, dry DMF, 100 °C, 50%; (d) piperidine cat., dry CH_3CN, 40 °C, 50%.

reaction. **DA-mPEG$_{750}$** is obtained starting from methoxypolyethylene glycol (**mPEG$_{750}$-OH**), which was chlorinated with $SOCl_2$ in $CHCl_3$ with pyridine as acid absorbing agent, followed by etherification with 4-diethylamino-2-hydroxybenzaldehyde in DMF using K_2CO_3 as base and KI (10% mol) as catalyst, respectively. Treatment **DA-mPEG$_{750}$** with 2-(3,5,5-trimethylcyclohex-2-en-1-ylidene) malononitrile, which is obtained by the condensation of isophorone with malononitrile in the catalyst of piperidine (1% mol), in CH_3CN provided target compound **TD-mPEG$_{750}$** in 50% yield. The chemical reagents and the reaction conditions are illustrated in Scheme 2, and the details of procedure for the preparation are described in Experimental Section.

3.2. Optical properties of *TD-mPEG$_{750}$* in solution

Absorbance and fluorescence of **TD-mPEG$_{750}$** (10 μM) in different solvents are measured at room temperature and photophysical data are reported in Table 1. **TD-mPEG$_{750}$** is composed with a D–π–A structure, which may exhibit intramolecular charge transfer characteristics. To confirm the intramolecular charge transfer of **TD-mPEG$_{750}$**, the linear optical properties of **TD-mPEG$_{750}$** in dilute solutions (10 μM) are measured and their photophysical data are reported in Table 1. In dimethyl sulfoxide (DMSO) solution (Fig. 1), **TD-mPEG$_{750}$** showed two main absorption bands at 325 nm and 555 nm, respectively, 325 nm may be deduced to a localized aromatic π → π* transition, and 555 nm to intramolecular charge transfer transition. Consistent with the predicted trend, the maximal absorption of **TD-mPEG$_{750}$** exhibits solvatochromic effect with different solvents, as shown in Table 1, the maximal absorption of **TD-mPEG$_{750}$** was blue-shifted from 555 nm

Table 1
Optical data of **TD-mPEG$_{750}$** in different solvents (10 μM) at 20 °C.

Solvent	λ_{max} (nm)	ε_{max} ($M^{-1}cm^{-1}$)	λ_{em}(nm)	Φ_f	Δλ (nm)
Toluene	517	2.4×10^4	597	0.04	80
DCM	531	2.6×10^4	633	0.035	102
CH_3CN	527	2.7×10^4	647	0.03	120
DMSO	555	2.8×10^4	662	0.06	107
H_2O	530	2.2×10^4	665	0.01	135

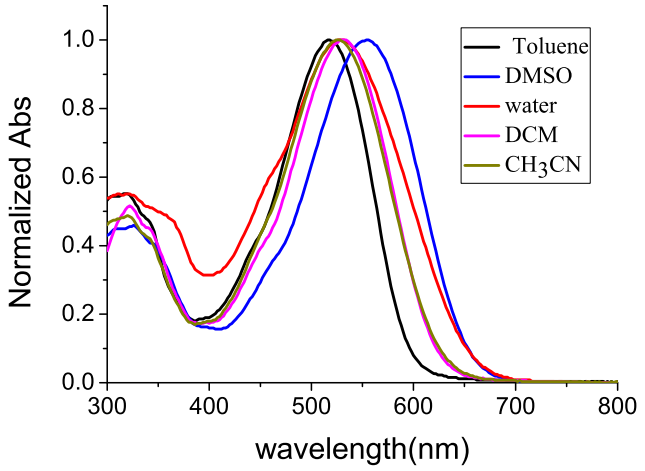

Fig. 1. Absorption spectral of **TD-mPEG$_{750}$** in different solvents (10 μM).

to 517 nm when the solvent was changed from DMSO (large polarity) to toluene (small polarity), which suggests a significant intramolecular charge transfer in solvent with large polarity.

Upon excitation the solution of **TD-mPEG$_{750}$** (10 μM) in DMSO solution with 560 nm light, a red fluorescence with the maximum emission wavelength at 662 nm is detected (Fig. 2), by using rubrene ($\phi_f = 0.27$, in MeOH) as reference [43], a small fluorescence quantum yield ($\phi_f = 0.06$) is obtained. Further investigation finds that **TD-mPEG$_{750}$** exhibits a positive solvatochromism: the emission wavelength is red-shifted with increase of the polarity of solvents. As shown in Table 1, the emission wavelength of **TD-mPEG$_{750}$** is red-shifted from 597 nm to 662 nm when the solvent is changed from toluene to DMSO. These positive solvatochromism properties are the characteristic of induced charge transfer in dipolar molecules. Besides, the fact that **TD-mPEG$_{750}$** presents more red-shifted in emission than that in absorption suggests there is stronger induced charge transfer in the excited state than in the ground state, which results in a large Stoke's shift ($\Delta\lambda \geq 100$ nm) in polar solvents. Fluorescence quantum yields of **TD-mPEG$_{750}$** in other solvents (Table 1) exhibit that the quantum yield increases with the increase of solvent viscosity (DMSO > toluene > DCM > acetonitrile) due to the restriction of vibronic deactivations in the excited state [44], which is in agreement with previous observations in this type of molecules [45].

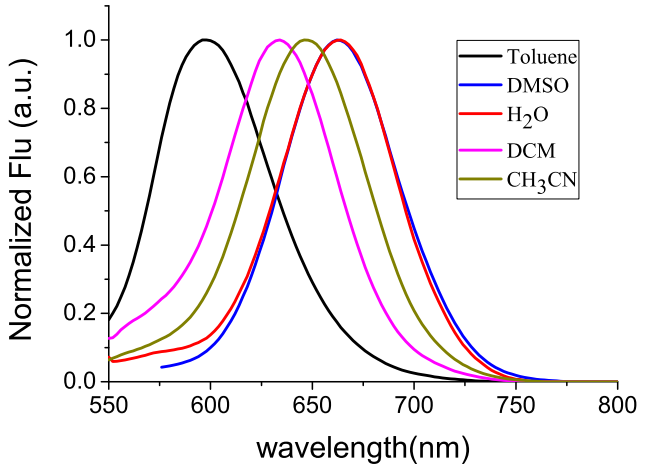

Fig. 2. Fluorescence spectral of **TD-mPEG$_{750}$** in different solvents (10 μM). $\lambda_{ex} = 530$ nm.

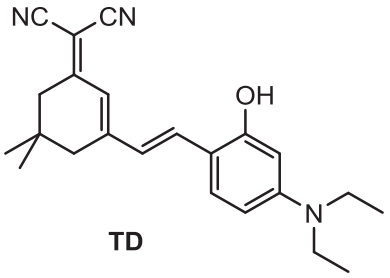

Scheme 3. Chemical structure of **TD**.

TD-mPEG$_{750}$ shows very weak emission in solution, which probably inherits from its parent compound **TD** (Scheme 3), it is found that **TD** also exhibits very weak emission in solution, and very small fluorescence quantum yield ($\phi_f = 0.05$) is obtained in DMSO solution [46]. The weak emission of this type of molecules is probably results from twisted intramolecular charge transfer (TICT) due to strong intramolecular charge transfer in excited state [47].

D–π–A conjugated ICT compounds are often highly polarized and generally suffer an aggregation-induced emission quenching. Since amphiphilic nature of **TD-mPEG$_{750}$**, it is necessary to understand whether **TD-mPEG$_{750}$** is molecular dissolved or aggregated state in water. Size and size distribution of **TD-mPEG$_{750}$** in H_2O (10 μM) were examined by dynamic light scattering (DLS) using DLS spectrometer (DynaPro NanoStar, Wyatt Technology) with a laser beam at a wavelength of 659 nm. The particle size measurements were performed at a scattering angle of 90° in a cell of 1.4 cm path length at room temperature (25 °C). DLS analyst confirmed that **TD-mPEG$_{750}$** formed aggregation in H_2O, as shown in Fig. 3, the particle size is about 32 nm with 70% number. The aggregation of **TD-mPEG$_{750}$** probably resulted in the decrease of emission in H_2O.

3.3. *Living cells fluorescence imaging*

TD-mPEG$_{750}$ applied for fluorescence imaging was explored. HeLa cells were incubated with **TD-mPEG$_{750}$** (1.0 μM) for 2 h, and the images of the live cells were taken by using a confocal laser scanning microscope (Fig. 4). The fluorescence images indicated that **TD-mPEG$_{750}$** was clearly expressed in HeLa cells. It is worth noting that a distinctly enhanced fluorescence was observed when **TD-mPEG$_{750}$** combined with HeLa cells, as a consequences, HeLa

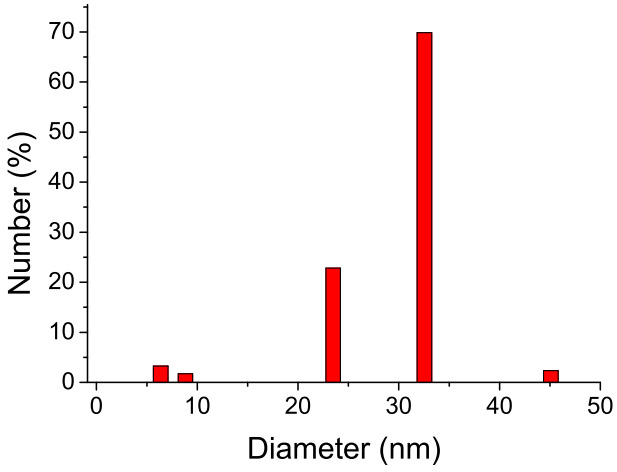

Fig. 3. Particle size and size distribution of **TD-mPEG$_{750}$** in H_2O (10 μM).

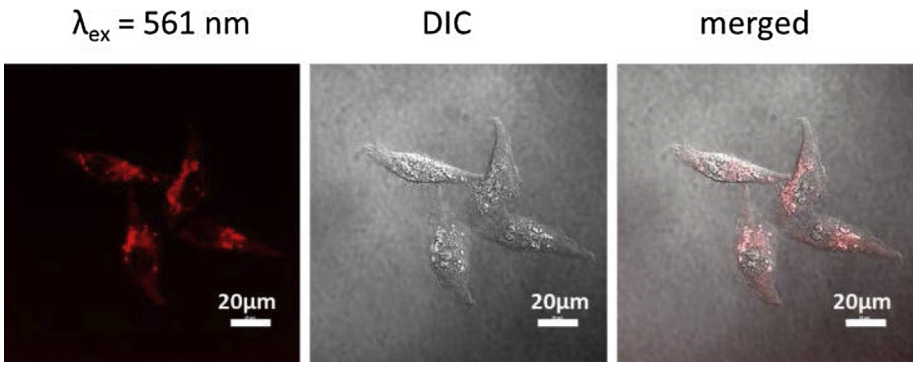

Fig. 4. Confocal laser scanning microscopic images of HeLa cells incubated with **TD-mPEG$_{750}$** (1.0 μM) (left).

cells incubated with **TD-mPEG$_{750}$** could be directly used for microscopic images without washing up by phosphate buffered saline (PBS). As presented in Fig. 4, no significant background interference was detected when the incubated HeLa cells was used for microscopic images without washing up.

To determine the cellular localization of **TD-mPEG$_{750}$**, the co-localization experiment with Mito-Tracker Green (Invitrogen) was preformed. HeLa cells were incubated with 1 μM of **TD-mPEG$_{750}$** for 2 h, followed by incubation with 25 nM of Mito-Tracker Green for 20 min. Both 488 nm and 561 nm excitation wavelength were employed for Mito-Tracker Green and **TD-mPEG$_{750}$**, respectively, and the fluorescence was recorded at channel (500–550 nm) and (570–620 nm), respectively. As presented in Fig. 5, the image with the probe is in good agreement with that of the commerical Mitro-Tracker Green, and the overlaid confocal fluorescence images of both **TD-mPEG$_{750}$** and Mito-Tracker Green demonstrated that **TD-mPEG$_{750}$** was expressed in mitochondria.

Discrimination against background fluorescence of HeLa cells was also conducted. Both fluorescence imaging from incubated HeLa cells with **TD-mPEG$_{750}$** and from background fluorescence imaging were obtained by using a confocal laser scanning microscope. As is demonstrated in Fig. 6, with excitation at 561 nm and recorded at channel (570–620 nm), both HeLa cells with and without incubation with **TD-mPEG$_{750}$** showed fluorescence signal, the auto-fluorescence of HeLa cells (middle) showed, however, much weaker than that of incubated HeLa cells (left), and a high contrast in fluorescence imaging was obtained (right). As shown in Fig. 6, the auto-fluorescence signal was hardly identified after the HeLa cells were incubated with **TD-mPEG$_{750}$**.

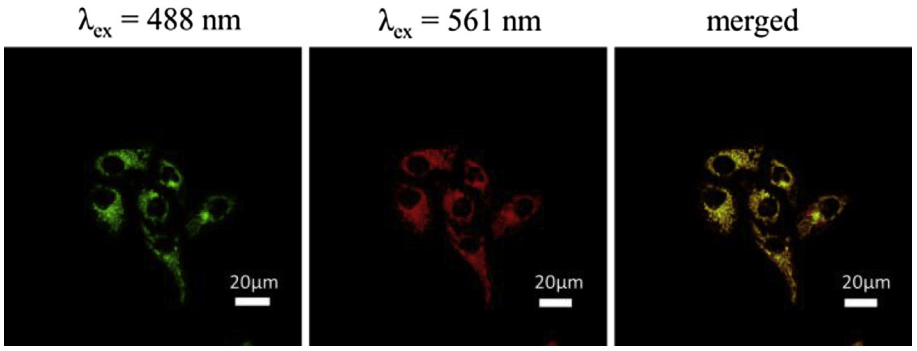

Fig. 5. Confocal laser scanning microscopic images of HeLa cells incubated with **TD-mPEG$_{750}$** (1.0 μM) (middle) and Mito-Tracker Green (left).

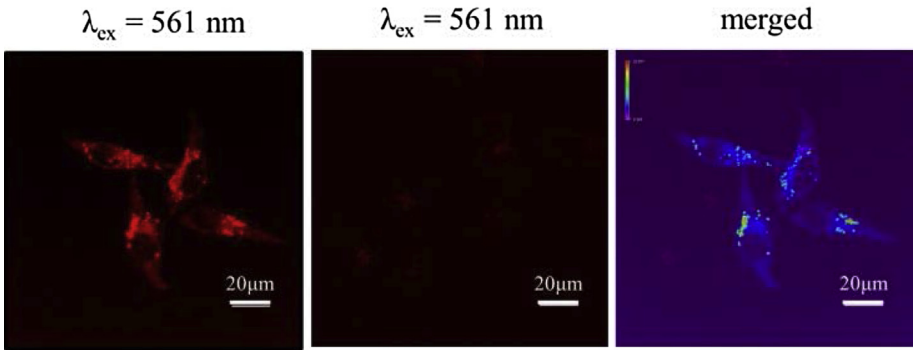

Fig. 6. Discriminating imaging against background fluorescence in HeLa cells (left: fluorescence imaging with incubation of **TD-mPEG$_{750}$** for 2 h, middle: background fluorescence imaging, right: merged fluorescence).

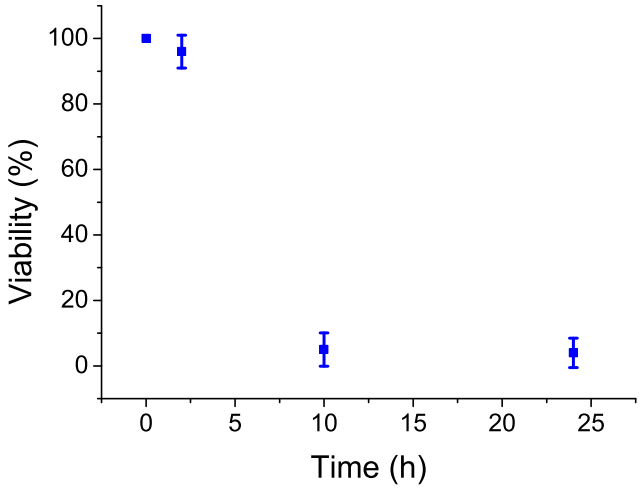

Fig. 7. The viability of HeLa cells with incubation of **TD-mPEG$_{750}$** (1.0 μM) for different time (error bar represents standard deviation).

3.4. Toxicity test of *TD-mPEG$_{750}$*

Toxicity is an important factor to evaluate the application possibility of fluorescence dyes. To test the cytotoxicity of **TD-mPEG$_{750}$**, propidium iodide (PI, Invitrogen, P3566), which is widely used in the toxicity study for identifying dead cells in a population, was employed as the probe for the detection of dead cells of HeLa. The HeLa cells incubated with **TD-mPEG$_{750}$** and PI probe were excited by 561 nm, and observed by Nikon A1R confocal fluorescence microscope with the fluorescence recorded at channel (670–720 nm) and (570–620 nm), respectively. The number of dead cells and the whole number of cells were counted from the obtained images, and the viability (%) (the ratio of living cells) was calculated by the comparison of the number of living cells with that of the dead cells. The result indicated that **TD-mPEG$_{750}$** showed moderate toxicity to HeLa cells, as shown in Fig. 7, more than 95% of viability was obtained when the HeLa cells were incubated with **TD-mPEG$_{750}$** within 2 h, but with the extension of time, the viability was decreased significantly, and less than 5% of viability was obtained when the HeLa cells were incubated with **TD-mPEG$_{750}$** more than 10 h.

4. Conclusions

In summary, a new water-soluble fluorescence dye based on dicyanoisophorone derivative has been developed and its application to living cells imaging has been demonstrated. The fluorescence dye has some distinct advantages including easy preparation, near-infrared emission ($\lambda_{em} \geq 650$ nm) and large Stoke's shift ($\Delta\lambda \geq 140$ nm), which is of benefit to biological fluorescence imaging.

Acknowledgments

This work was supported by the National Natural Science Foundation of China (No 91123032 and No 21302197).

References

[1] Oliveira Jr ON, Lost RM, Siqueira Jr JR, Crespilho FN, Caseli L. Nanomaterials for diagnosis: challenges and applications in smart devices based on molecular recognition. ACS Appl Mater Interfaces 2014;6:14745–66.
[2] Sandanaraj BS, Gremlich H, Kneuer R, Dawson J, Wacha S. Fluorescent nanoprobes as a biomarker for increased vascular permeability: implications in diagnosis and treatment of cancer and inflammation. Bioconjugate Chem 2010;21:93–101.
[3] Zhu C, Liu L, Yang Q, Lv F, Wang S. Water-soluble conjugated polymers for imaging, diagnosis, and therapy. Chem Rev 2012;112:4687–735.
[4] Lee S, Kang S, Ryu JH, Na JH, Lee D, Han SJ, et al. Tumor-homing glycol chitosan-based optical/PET dual imaging nanoprobe for cancer diagnosis. Bioconjugate Chem 2014;25:601–10.
[5] Wang J, Ye D, Liang G, Chang J, Kong J, Chen J. One-step synthesis of water-dispersible silicon nanoparticles and their use in fluorescence lifting imaging of living cells. J Mater Chem B 2014;2:4338–45.
[6] Egawa T, Hanaoka K, Koide Y, Ujita S, Takahashi N, Ikegaya Y, et al. Development of a far-red to near-infrared fluorescence probe for calcium ion and its application to multicolor neuronal imaging. J Am Chem Soc 2011;133:14157–9.
[7] Cho H, Alcantara D, Yuan H, Sheth RA, Chen HH, Huang P, et al. Fluorochrome-functionalized nanoparticles for imaging DNA in biological systems. ACS Nano 2013;7:2032–41.
[8] Zhang X, Zhang X, Yang B, Zhang Y, Wei Y. A new class of red fluorescent organic nanoparticles: noncovalent fabrication and cell imaging applications. ACS Appl Mater Interfaces 2014;6:3600–6.
[9] Lin CJ, Yang T, Lee C, Huang SH, Sperling RA, Zanella M, et al. Synthesis, characterization, and bioconjugation of fluorescent gold nanoclusters toward biological labeling applications. ACS Nano 2009;3:395–401.
[10] Chen J, Liu W, Zhou B, Niu G, Zhang H, Wu J, et al. Coumarin- and rhodamine-fused deep red fluorescent dyes: synthesis, photophysical properties, and bioimaging in vitro. J Org Chem 2013;78:6121–30.
[11] Miao J, Fan C, Sun R, Xu Y, Ge J. Optical properties of hemicyanines with terminal amino groups and their applications in near-infrared fluorescent imaging of nucleoli. J Mater Chem B 2014;2:7065–72.
[12] Wu J, Liu L, Matsuda T, Zhao Y, Rebane A, Dorbizhev M, et al. Improved orange and red Ca^{2+} indicators and photophysical considerations for optogenetic applications. ACS Chem Neurosci 2013;4:963–72.
[13] Walkup GK, Burdette SC, Lippard SJ, Tsien RY. A new cell-permeable fluorescent probe for Zn^{2+}. J Am Chem Soc 2000;122:5644–5.
[14] Haugland PR. Handbook of fluorescent probes and research chemicals. 6th ed. Eugene, OR: Molecular Probes, Inc.; 1996.
[15] Vazquez-Romero A, Kielland N, Arevalo MJ, Preciado S, Mellanby RJ, Feng F, et al. Multicomponent reactions for de novo synthesis of BODIPY probes: in vivo imaging of phagocytic macrophages. J Am Chem Soc 2013;135:16018–21.
[16] Weinstain R, Kanter J, Friedman B, Ellies LG, Baker ME, Tsien RY. Fluorescent ligand for human progesterone receptor imaging in live cells. Bioconjugate Chem 2013;24:766–71.
[17] Zhang H, Chen J, Guo X, Wang H, Zhang H. Highly sensitive low-background fluorescent probes for imaging of nitric oxide in cells and tissues. Anal Chem 2014;86:3115–23.
[18] Zhang X, Wang Z, Yue X, Ma Y, Kiesewetter DO, Chen X. pH-sensitive fluorescent dyes: are they really pH-sensitive in cells. Mol Pharm 2013;10:1910–7.
[19] Lu H, Mack J, Yang Y, Shen Z. Structural modifications strategies for the rational design of red/NIR region BODIPYs. Chem Soc Rev 2014;43:4778–823.
[20] Hoogendoorn S, Blom AE, Willems LI, van der Marel GA, Overkleeft HS. Synthesis of pH-activatable red fluorescent BODIPY dyes with distinct functionalities. Org Lett 2011;13:5656–9.
[21] Fu N, Xiong Y, Squier TC. Optimized design and synthesis of a cell-permeable biarsenical cyanine probe for imaging tagged cytosolic bacterial proteins. Bioconjugate Chem 2013;24:251–9.
[22] Lawson VA, Haigh CL, Roberts B, Kenche VB, Klemm HMJ, Masters CL, et al. Near-infrared fluorescence imaging of apoptotic neuronal cell death in a live animal model of prion disease. ACS Chem Neurosci 2010;1:720–7.
[23] Liu Y, Chen M, Cao T, Sun Y, Li C, Liu Q, et al. A cyanine-modified nanosystem for in vivo upconversion luminescence bioimaging of methylmercury. J Am Chem Soc 2013;135:9869–76.
[24] Cao H, Xiong Y, Wang T, Chen B, Squier TC, Uljana Mayer M. A red Cy3-based biarsenical fluorescent probe targeted to a complementary binding peptide. J Am Chem Soc 2007;129:8672–3.
[25] Koide Y, Urano Y, Hanaoka K, Terai T, Nagano T. Development of an Si-rhodamine-based far-red to near-infrared fluorescence probe selective for hypochlorous acid and its applications for biological imaging. J Am Chem Soc 2011;133:5680–2.
[26] Shibu ES, Ono K, Sugino S, Nishioka A, Yasuda A, Shigeri Y, et al. Photo-uncaging nanoparticles for MRI and fluorescence imaging in vitro and in vivo. ACS Nano 2013;7:9851–9.
[27] Wu X, Sun X, Guo Z, Tang J, Shen X, James TD, et al. In vivo and in situ tracking cancer chemotherapy by highly photostable NIR fluorescent theranostic prodrug. J Am Chem Soc 2014;136:3579–88.
[28] Laras Y, Hugues V, Chandrasekaran Y, Blanchard-Desce M, Acher FC, Pietrancosta N. Synthesis of quinoline dicarboxylic esters as biocompatible fluorescent tags. J Org Chem 2012;77:8294–302.
[29] Suchy M, Hudson RHE. Pyrimidine-fused heterocyclic frameworks based on an N4-arylcytosine scaffold: synthesis, characterization, and PNA oligomerization of the fluorescent cytosine analogue 5,6-benzopC. J Org Chem 2014;79:3336–47.
[30] Mohapatra M, Mishra AK. Photophysical behavior of fisetin in dimyristoylphosphatidylcholine liposome membrane. J Phys Chem B 2011;115:9962–70.

[31] Santos FS, Costa TMH, Stefani V, Goncalves PFB, Descalzo RR, Benvenutti EV, et al. Synthesis, characterization, and spectroscopic investigation of benzoxazole conjugated schiff bases. J Phys Chem A 2011;115:13390–8.
[32] Kitaoka M, Ichinose H, Goto M. Simultaneous visual detection of single-nucleotide variations in tuna DNA using DNA/RNA chimeric probes and ribonuclease A. Anal Biochem 2009;389:6–11.
[33] Redon S, Massin J, Pouvreau S, De Meulenaere E, Clays K, Queneau Y, et al. Red emitting neutral fluorescent glycoconjugates for membrane optical imaging. Bioconjugate Chem 2014;25:773–87.
[34] Wang L, Shen Y, Zhu Q, Xu W, Yang M, Zhou H, et al. Systematic study and imaging application of aggregation-induced emission of ester-isophorone derivatives. J Phys Chem C 2014;118:8531–40.
[35] Massin J, Charaf-Eddin A, Appaix F, Bretonniere Y, Jacquemin D, van der Sanden V, et al. A water soluble probe with near infrared two-photon absorption and polarity-induced fluorescence for cerebral vascular imaging. Chem Sci 2013;4:2833–43.
[36] Zhang X, Chen Y. Synthesis and fluorescence of dicyanoisophorone derivatives. Dyes Pigments 2013;99:531–6.
[37] Hou Y, Schoene CA, Regan KR, Munoz-Pinto D, Hahn MS, Grunlan MA. Photo-cross-linked $PDMS_{star}$-PEG hydrogels: synthesis, characterization, and potential application for tissue engineering scaffolds. Biomacromolecules 2010;11:648–58.
[38] Yu SS, Koblin RL, Zachman AL, Perrien DS, Hofmeister LH, Giorgio TD, et al. Physiologically relevant of xidative degradation of oligo(proline) cross-linked polymeric scaffolds. Biomacromolecules 2011;12:4357–66.
[39] Li Y, Wu H, Yang X, Jia M, Li Y, Huang Y, et al. Mitomycin C-soybean phosphatidylcholine complex-laded self-assembled PEG-lipid-PLA hybrid nanoparticles for targeted drug delivery and dual-controlled drug release. Mol Pharm 2014;11:2915–27.
[40] Yang J, Yan J, Zhuo Z, Amsden BG. Dithiol-PEG-PDLLA micelles: preparation and evaluatin as potentail topical ocular delivery vehicle. Biomacromolecules 2014;15:1346–54.
[41] Li J, Kao KJ. Synthesis of polyethylene glycol(PEG) derivatives and PEGylated-peptide biopolymer conjugates. Biomacromolecules 2003;4:1055–67.
[42] Diezi TA, Bae Y, Kwon GS. Enhanced stability of PEG-block-poly(N-hexyl stearate l-aspartamide) micelles in the presence of serum proteins. Mol Pharm 2010;7:1355–60.
[43] Boens N, Qin W, Basari N, Hofkens J, Ameloot M, Pouget J, et al. Fluorescence lifetime standards for time and frequency domain fluorescence spectroscopy. Anal Chem 2007;79:2137–49.
[44] Massin J, Dayoub W, Mulatieer JC, Aronica C, Bretonniere Y, Andraud C. Near-infrared solid-state emitters based on isophorone: synthesis, crystal structure and spectroscopic properties. Chem Mater 2011;23:862–73.
[45] Barsu C, Fortrie R, Nowika K, Baldeck PL, Vial JC, Barsella A, et al. Synthesis of chromophores combining second harmonic generation and two photon induced fluorescence properties. Chem Commun 2006;45:4744–6.
[46] Gao Z, Zhang X, Chen Y. Red fluorescence thin film based on a strong push-pull dicyanoisophorone system. Dyes Pigments 2015;113:257–62.
[47] Grabowski ZR, Rotkiewicz K. Structural changes accompanying intramolecular electron transfer: focus on twisted intramolecular charge-transfer states and structures. Chem Rev 2003;103:3899–4031.